JOURNAL OF GEOPHYSICAL RESEARCH, VOL. 101, NO. B9, PAGES 20,151-20,163, SEPTEMBER 10, 1996

Diurnal/semidiurnal polar motion excited by oceanic tidal angular momentum

B. F. Chao,[1] R. D. Ray,[2] J. M. Gipson,[3] G. D. Egbert,[4] and C. Ma[1]

Abstract. The axial component of the oceanic tidal angular momentum (OTAM) has been demonstrated to be responsible for most of the diurnal and semidiurnal variations in Earth's rotational rate. In this paper we study the equatorial components of OTAM and their corresponding effects on the orientation of Earth's rotational axis, or polar motion. Three ocean tide models derived from TOPEX/Poseidon satellite altimetry are employed to predict the polar motion excited by eight major diurnal/semidiurnal tides (Q_1, O_1, P_1, K_1, N_2, M_2, S_2, K_2). The predictions are compared with geodetic measurements of polar motion from both long-term observations and during the intensive campaign Cont94. The prograde diurnal and prograde and retrograde semidiurnal periods are treated, whereas the retrograde diurnal polar motion is not treated (because it cannot be observed directly and uniquely.) The comparison shows generally good agreement, with discrepancies typically within 10-30 micro-arc-seconds for the largest tides. The eight tides collectively explain nearly 60% of the total variance in subdaily polar motion during Cont94. This establishes the dominant role of OTAM in exciting the diurnal/semidiurnal polar motion and paves the way for detailed studies of short-period nontidal polar motion. The present accuracy, however, is inadequate to shed light on the prograde diurnal polar libration.

Introduction

Earth's rotation varies slightly with time due to geophysical processes that involve mass movement on or within the Earth. We say that these geophysical processes "excite" Earth rotational variations, which manifest themselves as changes in both the rotational speed and the rotational axis orientation. The scalar variation in the rotational speed is usually expressed in terms of the time derivative of the universal time UT1 (or often the length-of-day if the variation in question is longer than a day). The vectorial variation in the rotational axis orientation relative to the terrestrial reference frame is known as the polar motion.

One important excitation source is the luni-solar tides, as they influence Earth's rotation in a variety of ways [e.g., *Lambeck*, 1980]. The one under consideration here is the excitation via the conservation of angular momentum by the ocean tides. Two mechanisms are involved in this excitation process [e.g., *Munk and MacDonald*, 1960]: (1) tidal deformation in the form of tidal height variation that changes Earth's inertia tensor (referred to as the "mass" term); and (2) tidal motion represented by tidal current that evokes angular momentum relative to the solid Earth as a whole (referred to as the "motion" term). Connected by the conservation of mass, they are collectively called the oceanic tidal angular momentum (OTAM). In the presence of OTAM the conservation of the total angular momentum of the solid Earth-ocean system dictates changes in the solid Earth's rotation.

This paper compares the polar motion observed by the space geodetic techniques of very-long-baseline interferometry (VLBI) and satellite laser ranging (SLR), with model predictions of diurnal and semidiurnal OTAM derived from the TOPEX/Poseidon altimetry data [e.g., *Fu et al.*, 1994; *Le Provost et al.*, 1995]. At any given periodicity (such as tidal) the polar motion can be decomposed into the prograde and retrograde components (or "wobbles") [*Munk and MacDonald*, 1960]. Here we treat both components at the diurnal and semidiurnal periods, except the retrograde diurnal polar motion for which, for reasons described below, only the tide model predictions will be presented. In addition, results for UT1 that are updated from *Chao et al.* [1995] will be presented for comparison.

Polar Motion Excitation Dynamics

Both kinematic and dynamic complications set the polar motion problem apart from the UT1 problem. Kinematically,

[1]Laboratory for Terrestrial Physics, NASA Goddard Space Flight Center, Greenbelt, Maryland.
[2]Hughes STX, NASA Goddard Space Flight Center, Greenbelt, Maryland.
[3]NVI, Inc., NASA Goddard Space Flight Center, Greenbelt, Maryland.
[4]College of Oceanic and Atmospheric Sciences, Oregon State University, Corvallis.

Paper number 96JB01649.
0148-0227/96/96JB-01649$9.00

UT1 is a scalar quantity and all observers agree on its value independent of the reference frame. The rotational axis orientation, however, is a reference frame-dependent vectorial quantity: While methods that are sensitive to absolute rotation (such as those based on gravimetry or gyroscopic principles) can potentially make direct measurement of the "true" polar motion [*Chao*, 1991], present precise measurements of Earth rotation have been solely obtained from space geodetic techniques which measure the relative rotation. The space geodetic techniques do not determine the polar motion uniquely; instead, they observe the orientation of the celestial ephemeris pole [e.g., *Eubanks*, 1993; *Sovers et al.*, 1993; *Herring and Dong*, 1994]. As a result, the retrograde polar motion at the diurnal tidal periods is observationally aliased with and hence inseparable from the corresponding nutations. These terms are relatively large as they include the nutations driven by the external tidal torques and the polar motion resulting from the large solid Earth tides.

Dynamically, in contrast to the simple system function for UT1 excitation, the polar motion system function can be characterized by a linear oscillatory system with two distinct natural frequencies of resonance: the prograde Chandler wobble with a period of about 434 days, and the retrograde free core nutation (FCN) of the fluid core manifesting as a retrograde nearly diurnal free wobble with frequency -(1+1/430) cycle per sidereal day (cpsd) in the terrestrial frame [e.g., *Herring et al.*, 1986; *Merriam*, 1994]. In the retrograde diurnal band the near-resonance effect is very sensitive to the FCN period and Q [e.g., *Wahr*, 1981] (especially for components closest to FCN period such as K_1), so that detailed knowledge about the OTAM excitation of polar motion and nutation can in principle provide useful constraints on nutation models and the determination of FCN period and Q.

For the above two reasons, we shall not treat the retrograde diurnal polar motions per se in this paper but will only present the tide-height and current model predictions in this case.

The equation of motion for polar motion can be derived from the Liouville equation based on the conservation of angular momentum [*Munk and MacDonald*, 1960]. Written in the frequency (ω) domain, it is [*Sasao and Wahr*, 1981]

$$\mathbf{p}(\omega) = \left[1.124 \frac{\mathbf{h}(\omega)}{A\omega_0} + 0.772 \frac{\mathbf{c}(\omega)\omega_0}{A\omega_0} \right] * \frac{\omega_0}{\omega_{cw} - \omega} + \left[6.17 \times 10^{-4} \frac{\mathbf{h}(\omega)}{A\omega_0} + 0.0734 \frac{\mathbf{c}(\omega)\omega_0}{A\omega_0} \right] * \frac{\omega_0}{\omega_{fcn} - \omega} \quad (1)$$

where A is the Earth's equatorial moment of inertia, ω_0 is the mean angular rate of rotation, ω_{cw} is the positive Chandler angular frequency corresponding to prograde 434.45 sidereal days with a Q of 170 adopted from *Wilson and Vicente* [1990] (but see *Furuya and Chao* [1996]), and ω_{fcn} is the negative FCN angular frequency at -1.00232 cpsd, corresponding to retrograde 23.88 hours.

The complex-valued pole location $\mathbf{p}$ is given in radians; its real part is the x component along the Greenwich meridian, and its imaginary part is the y component along the 90°E longitude, in a right-handed terrestrial coordinate system. Its physical excitation consists of (1) the mass term: the complex-valued quantity $\mathbf{c}$ whose real and imaginary parts are the variation in the xz and yz components of the Earth's inertia tensor due to the mass redistribution; (2) the motion term: the complex-valued relative angular momentum $\mathbf{h}$ whose real and imaginary parts are simply the x and y components of the relative angular momentum. Here $\mathbf{c}\omega_0$ and $\mathbf{h}$ collectively represent the oceanic tidal angular momentum (OTAM). When normalized against $A\omega_0$ as expressed in equation (1), they represent the (dimensionless) excitation for the polar motion.

The first term in (1) arises from the Chandler wobble resonance. The numerical factors are the transfer functions [*Munk and MacDonald*, 1960] accounting for Earth's elastic yielding effect and the decoupling of the fluid core from the mantle. The second term arises from the FCN resonance. Except in the retrograde diurnal band near the resonance, its transfer functions are much smaller than their Chandler counterpart (especially for the motion term), so that the FCN term generally contributes much less to the polar motion excitation than the Chandler term, and possible errors in the FCN transfer functions become numerically unimportant.

The mass term $\mathbf{c}$ in OTAM arises from the tidal height, whereas the motion term $\mathbf{h}$ arises from the tidal current:

$$\mathbf{c}(t) = -a^4 \rho \int\int_{\text{ocean}} \zeta(\Omega,t) \sin\theta \cos\theta \, e^{i\lambda} \, d\Omega \quad (2a)$$

$$\mathbf{h}(t) = -a^3 \rho \int\int_{\text{ocean}} [u(\Omega,t)\cos\theta + iv(\Omega,t)] H(\Omega) e^{i\lambda} d\Omega \quad (2b)$$

In these equations, a is Earth's mean radius; $\rho = 1035$ kg m^{-3} is the mean density of seawater; Ω is an abbreviation for the colatitude θ and longitude λ; $d\Omega = \sin\theta d\theta d\lambda$ is the surface element for the integral over the oceans. The tidal height relative to the seabed is ζ; u and v are the eastward and northward speed, respectively, of the tidal current assumed to be barotropic and hence uniform over the water column with depth H. These tidal variables are provided by tide models described in the next section. Thus our study of polar motion proceeds by simple application of the principle of conservation of angular momentum; the nature of the torques that give rise to this motion need not concern us here.

Ocean Tide Convention and Models

To evaluate $\mathbf{c}(t)$ and $\mathbf{h}(t)$ of equation (2) requires global models of ocean tidal height and current fields. As is traditional, these models are decomposed into a set of discrete frequency components, or constituents, thus enabling evaluation of $\mathbf{c}(\omega)$ and $\mathbf{h}(\omega)$ in (1). This paper considers in detail the eight major diurnal and semidiurnal tidal constituents listed in Table 1 (Q_1, O_1, P_1, K_1, N_2, M_2, S_2, and K_2). Additional smaller tides are available from at least one of our analyses, and they may, in any event, be roughly inferred through admittance relationships [*Munk and Cartwright*, 1966].

This section discusses three global (or near-global) tide models and presents their implied estimates of polar motion

Table 1. Basic Properties of the Eight Major Diurnal and Semidiurnal Tides Studied in this Paper and the Free Core Nutation (FCN)

Tide	Period,	Alias Period,*	Doodson Argument**					Potential,***
(Type)	hours	days	τ	s	h	p	χ	cm
Diurnal								
Q_1 (L. elliptic)	26.868	9.13	1	-2	0	1	-90°	5.02
O_1 (L. princ.)	25.819	13.66	1	-1	0	0	-90°	26.22
P_1 (S. princ.)	24.066	182.62	1	1	-2	0	-90°	12.20
K_1 (S/L declin.)	23.935	∞	1	1	0	0	+90°	36.87
FCN	23.88	-430						-
Semidiurnal								
N_2 (L. elliptic)	12.658	9.13	2	-1	0	1	0°	12.10
M_2 (L. princ.)	12.421	13.66	2	0	0	0	0°	63.19
S_2 (S. princ.)	12.000	182.62	2	2	-2	0	0°	29.40
K_2 (S/L declin.)	11.967	∞	2	2	0	0	0°	7.99

Tide types L: lunar; S: solar.

* As observed in inertial space.

** Coefficients listed for the following angles: τ, mean lunar Greenwich time; s, mean longitude of Moon; h, mean longitude of Sun; p, mean longitude of lunar perigee. Note that if t is mean solar time, then $\tau = t - s + h$.

*** From *Cartwright and Tayler* [1971].

parameters. We begin, however, with a brief review of some tidal conventions; such a discussion appears warranted in so interdisciplinary a topic even though it will be well known to experts.

Tidal Phase Conventions

Along with the Kelvin-Darwin nomenclature for tidal constituents, Table 1 lists the tidal (cosine) arguments for the eight tides. These arguments imply use of standard phase conventions long used in oceanography [*Doodson*, 1921]. Unlike some other conventions, the Doodson arguments, when tabulated in numerical order, automatically classify the tides by species, group, and constituent, without overlap and in ascending order of frequency. (Recall that the classical definitions of a tidal species, group, and constituent are a set of tidal spectral lines whose first, first two, and first three Doodson numbers, respectively, are identical [*Doodson*, 1921; *Munk and Cartwright*, 1966]. Different species, groups, and constituents differ in frequency by at least 1 cycle/d, 1 cycle/month, and 1 cycle/yr, respectively.) The additional 90° increments in the diurnal band stem from Doodson's use of cosine for all terms of $(n+m)$ even but sine for $(n+m)$ odd, where m is species number (1 for diurnal, 2 for semidiurnal) and n is the spherical harmonic degree of the tidal potential (n=2 for all tides listed here). Finally, K_1 is 180° offset, because its amplitude in the harmonic development of the tidal potential [*Doodson*, 1921; *Cartwright and Tayler*, 1971] is of opposite sign relative to the other three diurnals. Direct allowance for this in the tidal argument ensures that tidal phase lags properly reflect the ocean's physically similar response to forcing at nearby frequencies; see, for example, our Tables 5 and 6 where phases vary smoothly across both the diurnal and semidiurnal bands.

Not shown in Table 1, but evident in expansions such as that of *Cartwright and Tayler* [1971], are the many additional smaller spectral lines comprising each tidal constituent. For the eight constituents listed, these lines occur significantly in only lunar tides; they differ in the fifth Doodson number (not shown), denoting dependence on the longitude of the lunar node and thus differing in frequency from the fundamental line by one or two cycles in 18.6 years. These nodal modulations are particularly important for O_1, K_1, and K_2. Obviously, they should be accounted for in any tidal analysis based on short time spans and in any tidal prediction. They have been rigorously accounted for in the ocean models discussed below. In VLBI and SLR analysis, authors have been inconsistent: some have and some have not allowed for them; fortunately, many of these space geodetic data sets are approaching two decades duration, so the neglect may not be so crucial.

One method of allowing for nodal modulations is to adopt the "nodal factor" F and U, which vary periodically with the lunar node [*Doodson and Warburg*, 1941] and are thus sensibly constant over periods of a few months. Any tidal constituent with amplitude A and phase lag G can then be expressed as $[A\,F(t)\cos(\boldsymbol{\beta}\cdot\boldsymbol{l}(t) + \chi + U(t) - G)]$, where $\boldsymbol{\beta}$ is a 4-vector of Doodson numbers and $\boldsymbol{l}(t)$ is a corresponding 4-vector of the astronomical variables in Table 1. This standard use of F and U assumes a constant tidal response for all lines within a constituent, which is sufficiently accurate for our purposes,

save one exception: retrograde diurnal lines near ω_{fcn}, where the resonance response in (1) violates this constant-admittance assumption. The above expression is followed in our tidal predictions of Figure 6 below, which does not include retrograde diurnal components.

Model predictions of tidal variations in polar motion follow from equations (1) and (2). The ω_{cw} and ω_{fcn} values we adopt for (1) follow *Gross* [1993] in order to facilitate comparison. Our phase convention for prograde and retrograde motions follows *Munk and MacDonald* [1960, equation (6.7.5)], and is consistent with *Gross* [1993]. The complex polar motion, corresponding to $\mathbf{p}(\omega)$ of (1), is written as

$$\mathbf{p}(t) = A_p \exp[\, i\alpha_p + i\phi(t)\,] + A_r \exp[\, i\alpha_r - i\phi(t)\,]$$

where $\phi(t)$ is the tidal argument as given in Table 1, and subscripts p and r indicate prograde and retrograde, respectively. Tables 6 and 7 will be in terms of the amplitudes A_p, A_r and phases α_p, α_r.

Ocean Tide Models

The three ocean models adopted here are based on analysis of the TOPEX/Poseidon (henceforth T/P) satellite altimetry measurements. T/P, launched in 1992 into a circular orbit of 66° inclination and 1336 km altitude, has generated a multiyear time series of open-ocean height measurements which, considering their near-global coverage, are of unprecedented accuracy, approximately 5 cm rms or less [*Fu et al.*, 1994]. The mission benefits from several improvements in altimetric technology, including use of a two-channel altimeter to compensate for ionospheric path delay and, mostly notably, tracking systems that have yielded radial orbit ephemerides accurate to approximately 3 cm rms [*Marshall et al.*, 1995]. A number of tidal analyses of T/P data have been carried out (several are described in the T/P special issue of *Journal of Geophysical Research, 99* (C12), 1994) [see also *Le Provost et al.*, 1995; *Andersen et al.*, 1995]. The three models adopted here, although relying on essentially the same altimetric data sets, employ different methodologies and are therefore complementary. The models are those by *Schrama and Ray* [1994] (version 9405, hereinafter referred to as model A), *Ray et al.* [1994b] (version 941230, hereinafter referred to as model B), and *Egbert et al.* [1994] (version TPXO.2, hereinafter referred to as model C). Briefly, both models A and B consist of tidal heights derived through strictly empirical analyses of the altimetric data, with tidal currents subsequently deduced by dynamical relationships; model C results from a form of data assimilation that yields simultaneously global fields of tidal heights and currents. Other models for which the tidal currents are not explicitly provided cannot be used for OTAM calculation.

For model A, *Schrama and Ray* [1994] applied simple harmonic fits to data captured in small bins covering the ocean surface, the bin size being dictated by considerations of tidal aliasing. The four major constituents M_2, S_2, K_1 and O_1 were determined in the form of corrections to the *Schwiderski* [1980] model. As with all three models, allowance was made for the fact that satellite altimeters are sensitive only to the geocentric tide: the sum of the ocean tide, the body tide, and the radial load tide. For the latter two, purely elastic models were adopted.

The tidal heights of model B were estimated with the response method [*Munk and Cartwright*, 1966], which determines the shape of the (complex) admittance across the diurnal and semidiurnal bands rather than the (complex) amplitudes of individual tidal constituents. The response method therefore yields essentially all major and minor tides within each band, although we use here only the eight constituents of Table 1. However, rather than quasi-independent analyses of binned data as in model A (and as in the Geosat investigation of *Cartwright and Ray* [1990] that did use the response method), model B expands each response weight as a series of special precomputed oceanic normal modes. This requires a large-scale global inversion (of 5300 estimated coefficients in the present case), but it results in more physically realistic smoothing of the tidal maps, dependent on the ocean bathymetry through the normal modes. The additional atmospheric forcing at the S_2 frequency was accounted for according to *Cartwright and Ray* [1994].

Following *Cartwright et al.* [1992], we estimate barotropic tidal currents for models A and B through hydrodynamical relationships with the height gradients. The method requires solving the following depth-averaged momentum equations (a modified form of Laplace's tidal equations) for u and v at each location at which current velocities are required:

$$\partial_t u - f v = -(g/a)\csc\theta\, \partial_\lambda(\zeta - \zeta_0 - \Upsilon) \qquad (3a)$$

$$\partial_t v + f u = (g/a)\, \partial_\theta(\zeta - \zeta_0 - \Upsilon) \qquad (3b)$$

where g is the mean surface gravitational acceleration, $f = 2\omega_0\cos\theta$ is the Coriolis parameter, ζ_0 is the "equilibrium" tide given by $(1+k_2-h_2)/g$ times the primary tidal potential, with the Love numbers k_2 and h_2 allowing for the elastic deformation of the body tide. The term Υ accounts for loading and self-attraction of the tide and is here computed through a high-degree spherical harmonic expansion (to degree 180) of the height field ζ [*Hendershott*, 1972].

Equations (3) contain no advection terms, no viscosity terms, in fact, no dissipative terms whatsoever. They are appropriate strictly to the deep ocean. This restriction is acceptable because even though shelf current velocities exceed deep-ocean velocities by 1 or 2 orders of magnitude, the small mass (shallow depth) associated with these currents implies that their angular momentum is of little importance (see below). Of course, in purely numerical hydrodynamical models of the tides, careful handling of dissipative mechanisms in shallow seas is crucial; here these mechanisms are implicit in our adopted (measured) height fields.

The right-hand sides of (3) are known once ζ is known. Velocity components u, v are then easily found, excepting at the critical latitudes $\sin^{-1}(\omega/2\omega_0)$, where $f = \omega$ and the equations are indeterminate, in fact, are essentially singular (because of physical approximations and measurement errors in the right-side terms). The critical latitudes for diurnal tides lie between 26.45° (for Q_1) and 30° (for K_1); for semidiurnal tides they lie

between 70.94° (for N_2) and 90° (for K_2). As *Cartwright et al.* [1992] discuss, if u and v are decomposed into rotary cyclonic and anticyclonic components, it is only the anticyclonic components that are indeterminate at the critical latitudes (stemming physically from the possible existence of inertial currents of identical frequency); the cyclonic components may be evaluated as usual. Test calculations show that the anticyclonic velocity estimates become unstable within about 5° of the critical latitudes. We have elected simply to interpolate the currents across the 10° gap. Less elementary approaches, invoking higher-order spatial gradients and Taylor series expansions, might overcome the critical latitude problem more accurately (G. W. Platzman, personal communication (1994), who points out an earlier discussion by *Brillouin* [1932]). We have not pursued this in any depth partly owing to the difficulties inherent in higher derivatives of measured (hence noisy) height fields. To our minds, assimilation methods hold more promise, and model C to which we now turn is an example.

Model C is derived using a generalized inverse or assimilation approach with a shallow-water hydrodynamic model [*Bennett*, 1992; *Egbert et al.*, 1994]. Tidal height and current fields are found by minimizing the misfit to both sea level elevations observed by T/P and the classical hydrodynamical equations of Laplace, including the equation of continuity and appropriate boundary conditions. For the dynamical constraints, linearized shallow water dynamics are assumed, essentially as in (3), but with an additional dissipation term incorporated as a linear parameterization of bottom drag. A simple scalar correction (similar to that of *Accad and Pekeris* [1978]) is used to account for ocean self attraction and load tides. The model domain extends farther north and south than the T/P coverage (see below), and all shallow continental shelf areas connected to the open ocean were included, to the extent possible with the roughly 2/3 degree grid. Details, including the relative weighting of dynamics and data, and the computational approach, are described by *Egbert et al.* [1994].

Unlike the methods of models A and B, the inverse methodology of model C provides a formal mechanism for computing error covariances and hence for placing standard errors on Earth rotation parameters. Work is in progress to accomplish this. For now, we must rely on model differences as the best guide to errors. In fact, given the difficulties of properly defining realistic covariances, including in inverse-theoretical approaches, reliance on differences of independent models is not necessarily a hindrance.

Nonetheless, the height fields of these models have been well studied. They have been compared among themselves and with other models, with in situ tide gauge and ocean bottom pressure measurements and with satellite altimeter measurements [*Andersen et al.*, 1995; C. K. Shum et al., Accuracy assessment of recent ocean tide models, submitted to *Journal of Geophysical Research*, 1996]. The comparisons suggest that the model A heights may be slightly more accurate than those of models B and C, but the differences are small, and all three models are considerably more accurate than any pre-T/P global model.

No detailed study of the current velocity fields has been undertaken. Yet we are confident that the model A currents are less accurate than those of model B or C, particularly in the diurnal band, because model A heights have more pronounced high-wavenumber noise (see the map of *Schrama and Ray* [1994]), which is compounded by the required spatial gradients of equation (3). The normal-mode and representer expansions of models B and C ensure that their heights are relatively smooth. In Table 2 we show a comparison of the model current velocities to reciprocal acoustic measurements in the Pacific Ocean by *Dushaw et al.* [1995] and to a current meter mooring of *Luther et al.* [1991]. (The quoted uncertainties in the acoustic and mooring measurements are between 0.3 and 0.5 mm s^{-1}.) Although this single comparison cannot replace a detailed global study, it does show that the model currents are sensibly realistic. A comparison between model C and tidal constants estimated using acoustic tomography data from the AMODE experiment in the Atlantic Ocean [*Dushaw et al.*, 1994] shows a similar level of agreement. There is also a suggestion that diurnal tides may be less accurate than semidiurnals.

Models A and B originally extended across only those latitudes overflown by T/P: 66°S to 66°N. Model C, by relying on hydrodynamic modeling, covered a slightly larger range: 80°S to 70°N. The three models are here supplemented in the

Table 2. Eastward Barotropic Current Velocity at 40.6°N, 163.0°W

	Diurnal Tides				Semidiurnal Tides			
	Q_1	O_1	P_1	K_1	N_2	M_2	S_2	K_2
Acoustic*	1, 64°	4, 101°	2, 132°	8, 128°	1, 191°	13, 223°	5, 272°	1, 268°
Current meter**	1, 110°	5, 122°	3, 141°	7, 135°	2, 216°	13, 218°	5, 280°	1, 280°
Model A	—	7, 149°	—	9, 126°	—	13, 226°	8, 272°	—
Model B	1, 104°	6, 116°	4, 135°	11, 135°	2, 225°	12, 216°	8, 265°	2, 263°
Model C	1, 95°	5, 110°	2, 129°	7, 131°	2, 193°	14, 219°	6, 271°	2, 275°

Amplitudes in mm s^{-1}, Greenwich phase lags in degrees. Model A from *Schrama and Ray* [1994], model B from *Ray et al.* [1994b], and model C from *Egbert et al.* [1994].

* From *Dushaw et al.* [1995], representing an average across a 745 km path.

** From *Luther et al.* [1991].

polar regions with tidal heights adopted from *Schwiderski* [1980] model for model A, from the strictly hydrodynamic model of *Le Provost et al.* [1994] for model B, and with tidal heights and currents from the hydrodynamic model of *Kowalik and Proshutinsky* [1994] for model C (major tides only). The reason for three different supplemental models is merely due to convenience and model availability during the course of the work. In any event, the polar regions, being small and located in extreme high latitudes, are found to contribute little to the polar motion excitation. A detailed treatment of the Arctic Ocean, including the handling of mass conservation as it affects tidal UT1, is given by *Ray et al.* [1996].

In Table 3 we tabulate the complete OTAM for all three components for the eight tides of Table 1, broken down to the mass term (height) and motion term (current) contributions. For space limitations we show only the results from model C. In a later section we list the vector totals of the polar motion excited by these OTAM for all models. For variations in UT1 the motion terms from tidal currents dominate the mass terms from tidal heights [*Baader et al.*, 1983; *Ray et al.*, 1994a]. Table 3 shows similar behavior for semidiurnal OTAM. The situation reverses for diurnal OTAM in x and y directions where the mass terms are generally, although not always, larger.

Before leaving the topic of model results, we also use the OTAM integrals of model C to investigate the influence of shallow seas and to justify the neglect of shallow-sea currents in models A and B. Table 4 shows the x and y OTAM components for the M_2 tide of model C, with and without the shallow seas. As expected, the currents in shallow areas contribute an insignificant amount to OTAM. Such is not the case for the tidal heights, however. Tidal heights in shallow water can be quite large, and they contribute appreciably to the inertia tensor. Unfortunately, tides in these regions are also complicated, varying rapidly with distance, and are not well mapped with altimetry. Shallow-water heights and deep-water currents are undoubtedly the primary sources of error in our tide-predicted polar motion.

Data Comparison Results

Polar Motion Data

As in work by *Chao et al.* [1995] (hereinafter referred to as CRE95), two types of polar motion data will be employed in comparisons with tide models: "long-term" and "intensive". The primary long-term data are based on multiyear observations from various VLBI networks, typically with 24-hour observing sessions separated by gaps of a few days. Independent algorithms have been applied to these raw data by various research groups [*Sovers et al.*, 1993; *Gipson et al.*, 1993; *Herring and Dong*, 1994; *Gipson*, 1996], resulting in spectral estimates of the diurnal/semidiurnal tidal parameters. Similar solutions from long-term SLR measurements to satellite LAGEOS are provided by R. Eanes (personal communication, 1996), which represent updated values from *Watkins and Eanes* [1994]. These estimates for the eight major diurnal and semidiurnal tides are given in Tables 5-7.

As for intensive observations of Earth rotation, there have been four VLBI special campaigns, each 1-2 weeks long: ERDE (October 15-31, 1989), Search92 (July 31 to August 9, 1992), Cont94 (January 12-26, 1994), and Cont95 (August 23-28, 1995). Sampling intervals as short as 1 hour are achieved. As in CRE95, the present paper will focus on Cont94 [*Gipson et al.*, 1994], because the formal errors during this intensive campaign were a factor of roughly 3 better than ERDE and a factor of 2 better than Search92. The formal errors during Cont95 are only slightly worse than those of Cont94, but the time span is shorter and the data processing is still preliminary at this writing. For the present purpose that focuses on subdaily variations, each day during Cont94 is analyzed independently; the agreement of the series across the daily boundaries serves as some indication of the goodness of the estimation.

UT1 Variation: An Update

First, we shall update the major results of CRE95 with respect to the diurnal/semidiurnal tidal UT1 variations with

Table 3. Oceanic Tidal Angular Momentum in All Three Components Broken down to the Mass (or Height) and Motion (or Current) Terms According to Model C

	Diurnal Tides				Semidiurnal Tides			
	Q_1	O_1	P_1	K_1	N_2	M_2	S_2	K_2
X								
Height	1.1, 342°	4.4, 334°	1.4, 316°	4.5, 312°	1.4, 349°	5.3, 12°	1.4, 50°	0.3, 53°
Current	0.8, 305°	3.4, 311°	1.5, 293°	5.1, 291°	1.5, 247°	10.7, 257°	5.8, 293°	1.5, 300°
Y								
Height	2.5, 218°	11.3,222°	4.3, 222°	13.5, 222°	0.4, 260°	4.3, 307°	3.3, 5°	0.9, 2°
Current	0.8, 209°	4.6, 207°	2.4, 192°	7.8, 188°	2.8, 160°	18.5, 167°	10.4, 199°	2.7, 199°
Z								
Height	0.8, 136°	2.3, 159°	0.4, 0°	1.5, 26°	0.8, 69°	6.3, 82°	2.8, 127°	0.9, 126°
Current	1.3, 106°	5.8, 119°	2.3, 125°	7.6, 125°	3.0, 326°	15.1, 318°	7.3, 344°	2.0, 336°

Amplitudes in 10^{24} kg m^2 s^{-1}; Greenwich phase lags in degrees.

Table 4. Oceanic Tidal Angular Momentum for M_2 According to Model C

	Mass Terms (Tidal Height)		Motion Terms (Tidal Current)	
	x	y	x	y
Global (minus Arctic Ocean)	5.76, 12.3°	4.23, 306.4°	10.36, 257.7°	18.31, 165.3°
No shallows (cutoff is 200 m)	5.36, 18.3°	3.43, 305.4°	10.39, 257.7°	18.31, 165.3°

Amplitudes in 10^{24} kg m^2 s^{-1}; Greenwich phase lags in degrees.

further findings within the present context. For comparison, two pre-T/P tide models will also be listed but without much discussion. One is based on the empirically constrained model of *Schwiderski* [1980]; its currents were calculated by *Cartwright et al.* [1992] (see also *Ray et al.* [1994a]) in the same manner as for models A and B. The other is the theoretical model by *Brosche et al.* [1989] followed by *Seiler* [1991], whose values were later reinterpreted by *Gross* [1993].

Table 5 augments Table 1 of CRE95 with two (yet unpublished) independent sets of estimates for UT1 excitation obtained from long-term SLR: that by R. J. Eanes (updated from *Watkins and Eanes* [1994], see above), and by *Pavlis* [1994]. The VLBI estimates according to *Gipson* [1996] also represents an improved set of values over those quoted in CRE95 based on work by *Gipson et al.* [1993], in that many more small tidal terms are included in the data reduction using the response method, and the nodal modulation is allowed for in O_1, K_1, M_2 and K_2.

Figure 1 examines the VLBI and SLR estimates of UT1 compared with T/P tide model predictions for the best determined tide M_2. It tells a more complicated story than presented in Figure 2 of CRE95. The latter, which is identical to Figure 1 here but without the two SLR estimates, showed that the M_2 spin libration [*Chao et al.*, 1991] can largely explain the departure of tide model predictions from VLBI estimates. However, now with the two SLR estimates lying on the other side of the model predictions, the discrepancies between tidal predictions and SLR estimates obviously cannot

Table 5. The UT1 Amplitudes and Greenwich Phase Lags for the Eight Diurnal and Semidiurnal Tides in Table 1

	Diurnal Tides				Semidiurnal Tides			
	Q_1	O_1	P_1	K_1	N_2	M_2	S_2	K
				Observations				
VLBI								
Sovers et al.	6.6, 37°	21.4, 39°	7.2, 27°	15.5, 13°	3.0, 221°	18.2, 235°	5.2, 266°	2.8, 251°
Herring/Dong	5.3, 36°	23.6, 47°	7.1, 34°	18.9, 20°	3.2, 240°	17.9, 233°	8.6, 269°	3.8, 282°
Gipson	5.6, 31°	22.2, 37°	5.8, 25°	18.6, 29°	3.7, 239°	18.6, 236°	8.0, 264°	2.9, 283°
SLR								
Eanes	7.0, 29°	22.6, 40°	5.8, 28°	18.2, 24°	3.5, 247°	17.0, 251°	9.6, 281°	2.7, 283°
Pavlis	5.0, 23°	25.2, 52°	6.6, 25°	22.7, 36°	4.6, 234°	18.8, 261°	4.2, 240°	3.3, 225°
				Predictions				
Brosche/Seiler*	—	35.2, 22°	7.1, 59°	18.7, 52°	7.5, 231°	35.3, 230°	18.1, 260°	—
Schwiderski**	4.3, 18°	20.4, 36°	5.9, 19°	21.2, 27°	3.6, 240°	18.7, 244°	7.7, 256°	1.9, 260°
TOPEX/Poseid								
Model A	—	20.5, 29°	—	22.3, 25°	—	19.4, 244°	7.7, 262°	—
Model B	4.8, 32°	23.2, 39°	8.3, 39°	24.2, 38°	3.8, 250°	17.6, 251°	7.7, 261°	2.1, 260°
Model C	5.6, 26°	20.1, 37°	5.9, 29°	19.7, 26°	4.1, 248°	17.7, 246°	7.6, 267°	2.0, 259°

Amplitudes in micro-seconds (μs); phase lags in degrees (see text for phase convention). The observations include those derived from long-term VLBI measurements and those from SLR. References: *Sovers et al.* [1993]; *Herring and Dong* [1994]; *Gipson*[1996]; *Eanes* [personal communication, 1996]; *Pavlis* [1994]; *Brosche et al.* [1989], *Seiler* [1991]; *Schwiderski* [1980]. The TOPEX/Poseidon predictions are computed according to T/P ocean tide models; model A from *Schrama and Ray* [1994], model B from *Ray et al.* [1994b], and model C from *Egbert et al.* [1994].

*As reinterpreted by *Gross* [1993].

**Tidal currents computed by *Cartwright et al.* [1992].

Table 6. Same as Table 5, but for the Prograde Polar Motion

	Diurnal Tides				Semidiurnal Tides			
	Q_1	O_1	P_1	K_1	N_2	M_2	S_2	K_2
				Observations				
VLBI								
Sovers et al.	49, 54°	132, 54°	69, 92°	134, 51°	23, 125°	22, 57°	21, 73°	32, 160°
Herring & Dong	35, 72°	199, 63°	60, 54°	152, 61°	17, 135°	58, 91°	12, 99°	39, 173°
Gipson	33, 81°	148, 74°	51, 60°	166, 63°	16, 108°	62, 110°	14, 89°	15, 104°
SLR								
Eanes	31, 81°	121, 71°	57, 65°	178, 66°	24, 144°	72, 117°	31, 110°	8.8, 115°
				Predictions				
Brosche/Seiler	—	181, 78°	55, 67°	172, 68°	22, 126°	105,	31, 68°	—
Schwiderski	29, 72°	142, 71°	54, 55°	179, 58°	22, 115°	81, 104°	24, 76°	6, 80°
TOPEX/Poseidon								
Model A	—	135, 76°	—	160, 65°	—	72, 111°	23, 82°	—
Model B	22, 82°	114, 67°	49, 57°	150, 57°	15, 127°	74, 120°	28, 86°	7, 90°
Model C	27, 77°	142, 70°	56, 63°	171, 63°	17, 135°	75, 116°	29, 86°	7, 96°

Amplitude in micro-arcseconds (μas).

be explained by spin libration. In fact, the two sets of estimates (VLBI and SLR), though agreeing relatively well within themselves, disagree by more than two standard deviations. This implies the presence of significant systematic errors in at least one set of observations, and possibly both, due possibly to inadequate tidal loading corrections at ground station sites. The resolution of this matter awaits further research.

Figure 6a replots the predicted UT1 curve of T/P models B and C, superimposed on the hourly Cont94 data from the NASA R&D network as in Figure 1 of CRE95, except that

Table 7. Same as Table 6, but for the Retrograde Polar Motion

	Diurnal Tides				Semidiurnal Tides			
	Q_1	O_1	P_1	K_1	N_2	M_2	S_2	K_2
				Observations				
VLBI*								
Sovers et al.	—	—	—	—	37, 267°	265, 273°	174, 303°	62, 286°
Herring & Dong	—	—	—	—	48, 282°	265, 272°	120, 304°	31, 328°
Gipson	—	—	—	—	46, 269°	257, 272°	128, 303°	18, 346°
SLR*								
Eanes	—	—	—	—	28, 253°	253, 267°	124, 297°	33, 301°
				Predictions				
Brosche/Seiler	—	83, 201°	881, 153°	8865, 148°	40, 249°	303, 240°	232, 287°	—
Schwiderski	39, 304°	142, 305°	804, 139°	9400, 135°	35, 267°	251, 278°	135, 303°	38, 306°
TOPEX/Poseidon								
Model A	—	167, 305°	—	9510, 129°	—	245, 271°	121, 298°	—
Model B	68, 321°	200, 314°	838, 138°	9700, 135°	46, 267°	262, 274°	140, 303°	40, 301°
Model C	45, 307°	132, 297°	797, 136°	9670, 133°	45, 269°	263, 271°	131, 298°	34, 301°

*The observed retrograde diurnal values are absent for the reasons given in the text.

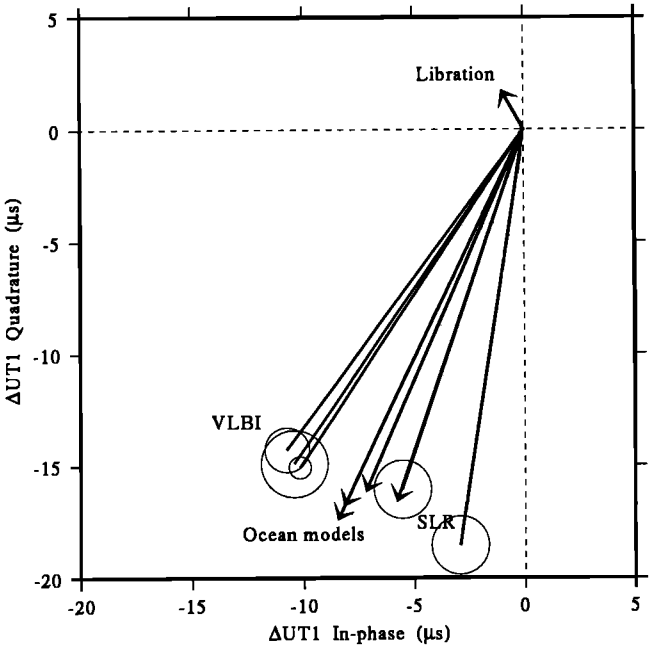

Figure 1. The phasor diagram for UT1 variation at the M_2 period: Three VLBI- and two SLR-observed values (with formal error circles), and four tide-model predictions (three T/P models, as well as the Schwiderski model which will not be shown in Figures 2-5) are given according to Table 5. The corresponding contribution of the Earth spin libration is also plotted.

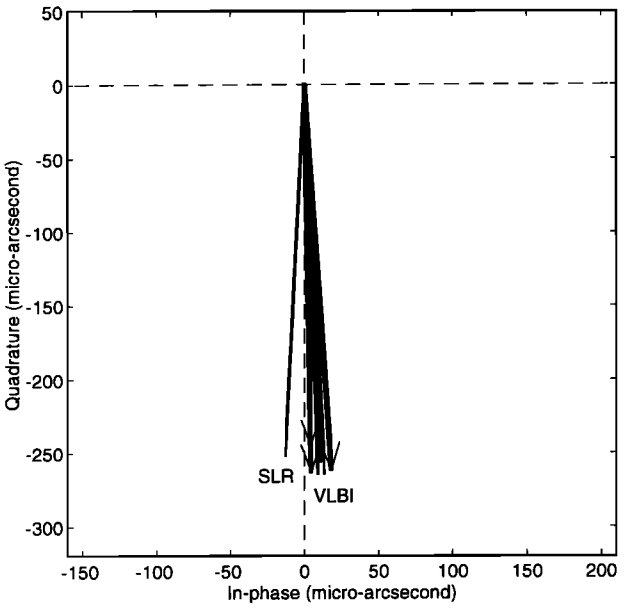

Figure 2. The phasor diagram for the retrograde M_2 polar motion according to Table 7: Three VLBI- and one SLR-observed values are given as thin lines properly labeled. The three T/P tide model predictions are shown as the heavy arrows. Consult Table 7 for individual identifications.

here the Cont94 data are preprocessed in a procedure somewhat improved from those in CRE95, and the NEOS network data used in CRE95 in extending the series and filling the 1-day gap are not included here. The processing adopted here gives slightly better agreement with the tidal models than presented in CRE95.

Polar Motion: "Long-Term" Comparison

Tables 6 and 7 list the prograde and retrograde polar motion, respectively, for the eight diurnal/semidiurnal tide constituents. Figures 2-5 plot the phasor diagrams for some of the better determined tides with polar motion amplitudes exceeding 100 micro-arcseconds (μas), or about 3 mm in pole position. On each diagram, three T/P tide model predictions (the heavy arrows, consult Tables 6 and 7 for individual identification), three VLBI estimates, and one SLR estimate are shown (and so labeled). The separation between estimates indicates the uncertainties associated with each type of estimate.

Several facts are noted as follows:

1. The large amplitudes in the model-predicted retrograde diurnal components due to FCN resonance are listed here only for reference. As discussed earlier, no direct observations for them are available. The largest amplitudes depend sensitively on the actual FCN period and Q.

2. In general, the three T/P tide models agree well in their polar motion predictions, typically within 5-10 μas in amplitude and 10° in phase. This is consistent with findings in CRE95 for UT1.

3. The agreement between T/P tide-model predictions and observations is generally fairly good, especially for tides with relatively large amplitude. The best determined component is retrograde M_2; the agreement is within several percent, or typically 10 μas. The next largest component, prograde K_1, also sees agreement within about 15%, or some 20 μas. Overall, the best agreement is found between VLBI estimates by *Gipson* [1996] and T/P model C predictions.

4. The agreement is poorer for smaller tides. This is also true among the VLBI estimates; *Sovers et al.* [1993] differ with others for the prograde M_2 and retrograde K_2 by up to a factor of 3, and less severely for the retrograde S_2 and prograde K_1. The reason may be related to the internal inconsistency among Sovers et al.'s estimates for these tides obtained from different VLBI networks.

5. There are often systematic differences between VLBI and SLR estimates. The most notable case is the prograde K_2, where two of the three VLBI estimates have anomalously large amplitudes (judging from the small tidal potential for this tide in Table 1) and diverse phases. *Gipson*'s [1996] VLBI estimate for this tide is much less anomalous, while the SLR estimate agrees much better with model predictions.

6. The Schwiderski model (with *Cartwright et al.* [1992] currents) agrees well with the T/P models in their polar motion predictions, whereas the Brosche/Seiler model often predicts a much larger effect. This is also found to be the case for UT1 by *Ray et al.* [1994a]. The accuracy of Schwiderski model is somewhat surprising, given that the T/P elevation models are significantly more accurate (Shum et al., submitted manuscript,

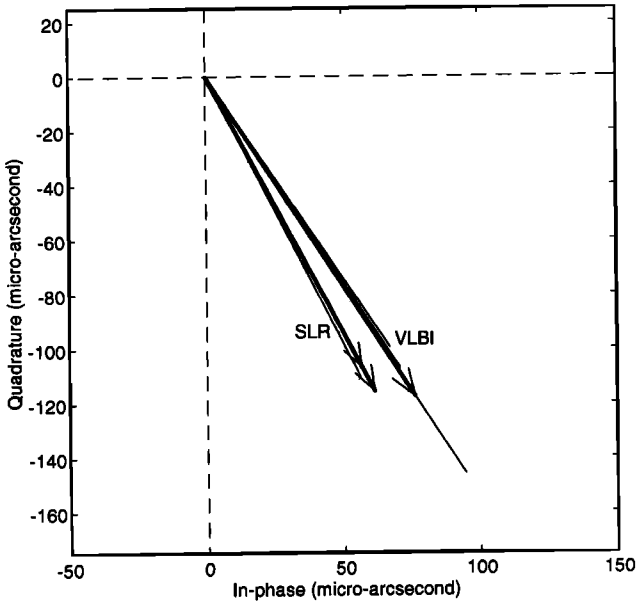

Figure 3. Same as Figure 2 but for retrograde S_2 polar motion.

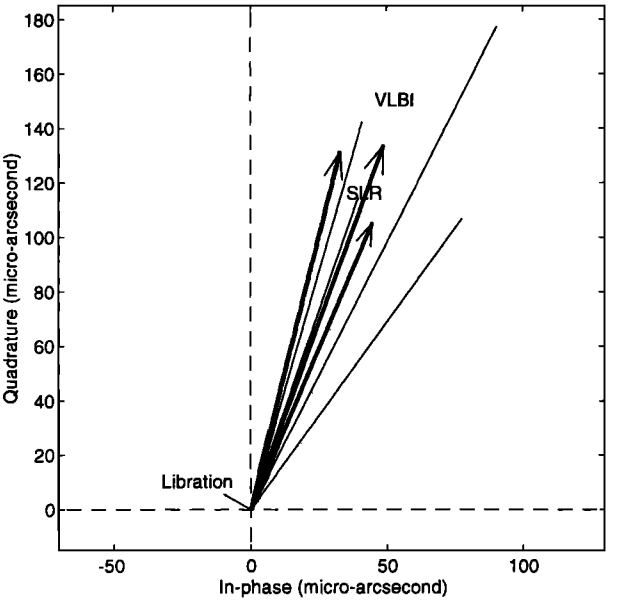

Figure 5. Same as Figure 4 but for prograde O_1 polar motion.

1996). The reason for this presumably lies in certain fortuitous cancellation of the errors when the model is integrated to form the Earth rotation parameters.

Polar Motion: "Intensive" Comparison

Figures 6b and 6c present the hourly data of the x and y components of polar motion during Cont94 intensive campaign. Superimposed on them are the predicted curves of T/P models B and C (model A is not plotted because it has fewer tide constituents).

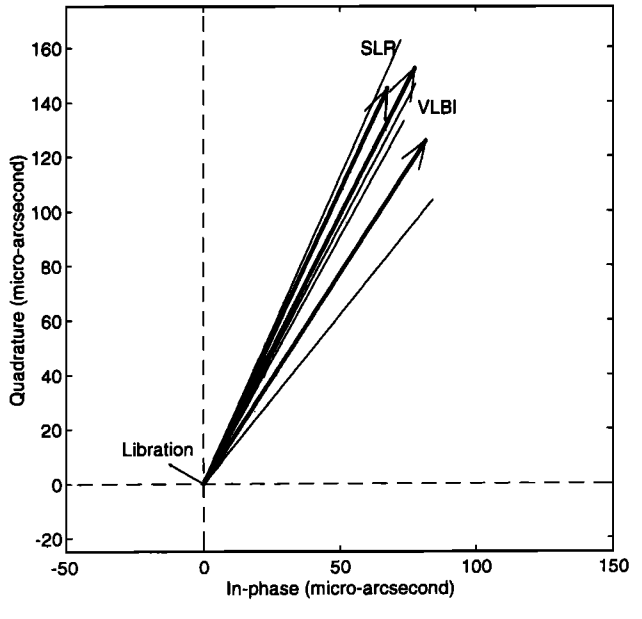

Figure 4. Same as Figure 2 but for prograde K_1 polar motion according to Table 6. The corresponding contribution of the Earth polar libration is also plotted. Consult Table 6 for individual identifications.

The match between model predictions and observations is apparently quite good, although not as good as the top panel for UT1. This match can be quantified as follows. The total variance of the Cont94 polar motion series (in its complex form) is found to be 215 in units of 10^3 μas^2, while the noise variance given the formal error [*Gipson et al.*, 1994] is about 26. As expected, we find the total variance greatly reduced, to 110, after subtraction of the tides (themselves of variance 122 according to model C). Therefore, assuming uncorrelated noise, approximately 1-(110-26)/(215-26) or nearly 60% of the subdaily polar motion power can be explained by the eight tides (compared to the corresponding ~90% for UT1). This on one hand establishes the dominant role of tides in exciting subdaily polar motion, and on the other hand indicates the existence of important nontidal contributions. Besides observational noises and modeling errors, the majority of the discrepancies seen in Figure 6 can presumably be attributed to the following effects not considered in the ocean tide models: (1) the presence of other geophysical sources such as subdaily atmospheric and oceanic angular momentum variations, daily and half-daily atmospheric thermal "tides," Earth librations (see below), and possibly earthquakes; (2) contributions from the response of the internal inhomogeneities of the solid Earth to diurnal and semidiurnal tidal forcing; (3) the neglect of smaller tides in the tide models presented here [cf. *Seiler and Wünsch*, 1995]. Closer examination of Figure 6 shows that the tide models almost always underpredict the diurnal and especially the semidiurnal peaks. This is true for both UT1 (see CRE95) and polar motion. Similar phenomenon is found with respect to Cont95 data as well [*Gipson et al.*, 1996]. The initial study by *Ma et al.* [1995] has indicated the importance of the atmospheric angular momentum and thermal tides; but, clearly, more comprehensive investigations will be needed.

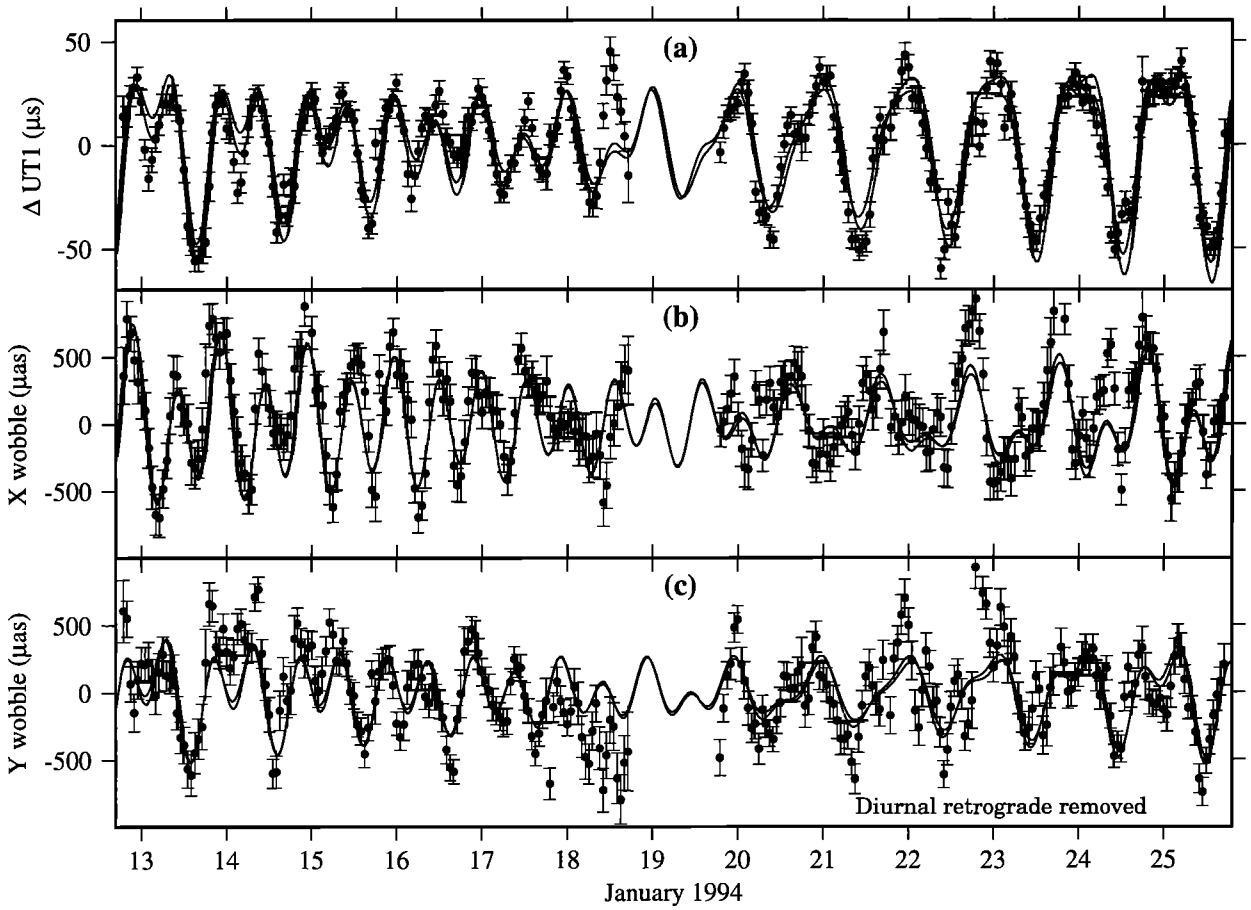

Figure 6. Comparison of Earth rotation variations during Cont94 Campaign. The hourly observations with standard errors are those made by VLBI (the NASA R&D network); the solid lines are predictions according to T/P tide Models B and C (see text). (a) UT1 variation in units of μs; (b) x and (c) y components of the polar motion (in units of μas) without the retrograde diurnal components.

Polar Libration

Besides the semidiurnal spin librations (discussed above), the luni-solar tidal torques exerted on Earth's equatorial ellipticity give rise to diurnal polar librations in the prograde direction [*Chao et al.*, 1991]. The observed polar motion should contain the tide-generated polar motion and the polar librations, the largest amplitude of which (for K_1) is probably no more than 15 μas depending on the interior properties of the Earth. Thus, if sufficiently accurate, the observed and tide-generated polar motion can be differenced to reveal the libration contribution. One hopes that this will lead to useful constraints on Earth's interior properties, particularly the equatorial ellipticity of the core-mantle boundary [*Chao et al.*, 1991; *Herring and Dong*, 1994; CRE95].

According to formulae given by *Chao et al.* [1991] under the present phase convention, the predicted polar libration is (14.6 μas, 150°) for K_1 and (11.3 μas, 150°) for Q_1 as plotted in Figures 4 and 5, respectively. Unfortunately, the departures within estimates from each technique, and hence the estimation uncertainties, are generally larger than the libration. Thus, similarly for UT1, the present measurement and modeling accuracies are inadequate for the libration to "close" the budget even for the largest tidal polar motions.

Summary

The oceanic tidal angular momentum (OTAM), consisting of the mass and motion terms, excites Earth rotation variation at all tidal periods. CRE95 established that the axial component of OTAM is responsible for as much as 90% of the subdaily (primarily diurnal and semidiurnal) power of the UT1 variation. Here updated examples are presented in Figures 1 and 6a. The main purpose of the present paper, however, is to study the equatorial components of OTAM and their corresponding effects on the polar motion.

The equatorial components of OTAM for eight major diurnal/semidiurnal tides (Q_1, O_1, P_1, K_1, N_2, M_2, S_2, K_2) are computed according to three ocean tide models derived from TOPEX/Poseidon satellite altimetry. Agreeing well among themselves, these predictions are then compared with geodetic measurements of polar motion made by VLBI and SLR long-term observations as well as VLBI intensive measurements during the Cont94 campaign. The prograde diurnal and

prograde and retrograde semidiurnal polar motions are treated; the retrograde diurnal polar motion is not treated because it cannot be observed directly and independently of the nutations by geodetic means.

The comparison shows generally good agreement, with discrepancies typically within 10-30 μas for the largest tides and progressively poorer for smaller tides. Examples are given in Figures 2-5. Overall, the best agreement is found between VLBI estimates by *Gipson* [1996] and tide model predictions according to T/P model of *Egbert et al.* [1994]. During the 2 weeks of Cont94, the eight tides collectively explain nearly 60% of the total variance in sub-daily polar motion, as shown in Figures 6b and 6c. This on one hand establishes the dominant role of OTAM in exciting the diurnal/semidiurnal polar motion and on the other hand paves the way for detailed studies of nontidal polar motion. The excitation sources for the latter include subdaily atmospheric and oceanic angular momentum variations, the daily and half-daily atmospheric thermal "tides", Earth librations, earthquakes, and the response of the internal inhomogeneities of the solid Earth to diurnal/semidiurnal tidal forcing. A full, quantitative resolution awaits further data and investigations.

Acknowledgments. We thank E. Pavlis and R. Eanes for the unpublished SLR results. This work is supported by the NASA Geophysics Program.

References

Accad, Y., and C. L. Pekeris, Solution of the tidal equations for the M_2 and S_2 tides in the world oceans from a knowledge of the tidal potential alone, *Philos. Trans. R. Soc. London, 290*, 235-266, 1978.

Andersen, O. B., P. L. Woodworth, and R. A. Flather, Intercomparison of recent ocean tide models, *J. Geophys. Res., 100*, 25,261-25,282, 1995.

Baader, H. R., P. Brosche, and W. Hövel, Ocean tides and periodic variations of the Earth's rotation, *J. Geophys., 52*, 140-142, 1983.

Bennett, A. F., *Inverse Methods in Physical Oceanography*, Cambridge Univ. Press, New York, 1992.

Brillouin, M., Marées dynamiques: Les latitudes critiques, *C. R. Acad. Sci., 194*, 801-804, 1932.

Brosche, P., U. Seiler, J. Sundermann, and J. Wünsch, Periodic changes in Earth's rotation due to oceanic tides, *Astron. Astrophys., 220*, 318-320, 1989.

Cartwright, D. E., and R. D. Ray, Oceanic tides from Geosat altimetry, *J. Geophys. Res., 95*, 3069-3090, 1990.

Cartwright, D. E., and R. D. Ray, On the radiational anomaly in the global ocean tide, with reference to satellite altimetry, *Oceanologica Acta, 17*, 453-459, 1994.

Cartwright, D. E., and R. J. Tayler, New computations of the tide-generating potential, *Geophys. J. R. Astron. Soc., 23*, 45-74, 1971.

Cartwright, D. E., R. D. Ray, and B. V. Sanchez, A computer program for predicting oceanic tidal currents, *NASA Tech. Memo., TM-104578*, 1992.

Chao, B. F., As the world turns, II, *EOS Trans. AGU, 72*, 550–551, 1991.

Chao, B. F., D. N. Dong, H. S. Liu, and T. A. Herring, Libration in the Earth's rotation, *Geophys. Res. Lett., 18*, 2007–2010, 1991.

Chao, B. F., R. D. Ray, and G. D. Egbert, Diurnal/semidiurnal oceanic tidal angular momentum: TOPEX/Poseidon models in comparison with Earth's rotation rate, *Geophys. Res. Lett. 22*, 1993-1996, 1995.

Doodson, A. T., The harmonic development of the tide-generating potential, *Proc. R. Soc. London A, 100*, 305-329, 1921. (Reprinted in *Int. Hydrog. Rev., 31*, 11-35, 1954.)

Doodson, A. T., and H. D. Warburg, *Admiralty Manual of Tides*, His Majesty's Station Off., London, 1941.

Dushaw, B. D., P. F. Worcester, B. D. Cornuelle, and B. M. Howe, Barotropic and baroclinic tides of the western North Atlantic, *Eos Trans. AGU, 75* (44), Fall Meet. Suppl., 307, 1994.

Dushaw, B. D., B. D. Cornuelle, P. F. Worcester, B. M. Howe, and D. S. Luther, Barotropic and baroclinic tides in the central North Pacific Ocean determined from long-range reciprocal acoustic transmissions, *J. Phys. Oceanogr., 25*, 631-647, 1995.

Egbert, G. D., A. F. Bennett, and M. G. G. Foreman, TOPEX/Poseidon tides estimated using a global inverse model, *J. Geophys. Res., 99*, 24,821-24,852, 1994.

Eubanks, T. M., Variations in the orientation of the Earth, in *Contributions of Space Geodesy to Geodynamics: Earth Dynamics, Geodyn. Ser.*, vol. 24, edited by D. E. Smith and D. L. Turcott, pp. 1-54, AGU, Washington, D. C., 1993.

Fu, L. L., E. J. Christensen, C. A. Yamarone, M. Lefebvre, Y. Menard, M. Dorrer, and P. Escudier, TOPEX/Poseidon mission overview, *J. Geophys. Res., 99*, 24,369-24,381, 1994.

Furuya, M., and B. F. Chao, Estimation of period and Q of the Chandler wobble, *Geophys. J. Int.*, in press, 1996.

Gipson, J. M., VLBI determination of neglected tidal terms in high-frequency Earth orientation variation, *J. Geophys. Research*, in press, 1996.

Gipson, J. M., B. F. Chao, and C. Ma, Rapid EOP variations measured by VLBI, *Eos Trans. AGU, 74* (16), Spring Meet. Suppl., 103, 1993.

Gipson, J. M., C. Ma, T. M. Eubanks, and A. P. Freedman, Diurnal and subdiurnal EOP variations during CONT94, *Eos Trans. AGU, 75* (16), Spring Meet. Suppl., 111, 1994.

Gipson, J. M., C. Ma, R. D. Ray, and B. F. Chao, Continuous Earth-Orientation Parameter Measurements by VLBI, *Eos Trans. AGU, 77* (17), Spring Meet. Suppl., S44, 1996.

Gross, R. S., The effect of ocean tides on the Earth's rotation as predicted by the results of an ocean tide model, *Geophys. Res. Lett., 20*, 293-296, 1993.

Hendershott, M. C., The effects of solid Earth deformation in global ocean tides, *Geophys. J. R. Astron. Soc., 29*, 389-402, 1972.

Herring, T. A., and D. Dong, Measurement of diurnal and semidiurnal rotational variations and tidal parameters of Earth, *J. Geophys. Res., 99*, 18,051-18,071, 1994.

Herring, T. A., C. R. Gwinn, and I. I. Shapiro, Geodesy by radio interferometry: Studies of forced nutations of the Earth, 1, Data analysis, *J. Geophys. Res., 91*, 4745-4754, 1986.

Kowalik, Z., and A. Y. Proshutinsky, The Arctic Ocean tides, in *The Polar Oceans and Their role in Shaping the Global Environment, Geophys. Monogr. Ser.*, vol. 85, edited by O. M. Johannessen, R. D. Muemch, and J. E. Overland, pp. 137-158, AGU, Washington, D.C., 1994.

Lambeck, K., *The Earth's Variable Rotation*, Cambridge Univ. Press, New York, 1980.

Le Provost, C., M. L. Genco, F. Lyard, P. Vincent, and P. Canceil, Spectroscopy of the world ocean tides from a finite element hydrodynamic model, *J. Geophys. Res., 99*, 24,777-24,797, 1994.

Le Provost, C., A. F. Bennett, and D. E. Cartwright, Ocean tides for and from TOPEX/Poseidon, *Science, 267*, 639-642, 1995.

Luther, D. S., J. H. Filloux, and A. D. Chave, Low frequency motionally induced electromagnetic fields in the ocean, 2, Electric field and Eulerian current comparison, *J. Geophys. Res., 96*, 12,797-12,814, 1991.

Ma, C., B. F. Chao, J. M. Gipson, D. J. Steinberg, and R. D. Ray,

Correlation of atmospheric angular momentum and VLBI Earth orientation at periods below two weeks, paper presented at IUGG XXI General Assembly, Boulder, 1995.

Marshall, J. A., N. P. Zelensky, S. M. Klosko, D. S. Chinn, S. B. Luthcke, K. E. Rachlin, and R. G. Williamson, The temporal and spatial characteristics of the TOPEX/Poseidon radial orbit error, *J. Geophys. Res., 100,* 25,331-25,352, 1996.

Merriam, J. B., The nearly diurnal free wobble resonance in gravity measured at Cantley, Quebec, *Geophys. J. Int., 119*, 369-380, 1994.

Munk, W. H., and D. E. Cartwright, Tidal spectroscopy and prediction, *Philos. Trans. R. Soc. London A, 259,* 533-581, 1966.

Munk, W. H., and G. J. F. MacDonald, *The Rotation of the Earth,* Cambridge Univ. Press, New York, 1960.

Pavlis, E. C., Origin and orientation variations of the terrestrial frame observed from LAGEOS, *Eos Trans. AGU, 75* (44), Fall Meet. Suppl., 62, 1994.

Ray, R. D., D. J. Steinberg, B. F. Chao, and D. E. Cartwright, Diurnal and semidiurnal variations in the Earth's rotation rate induced by oceanic tides, *Science, 264*, 830-832, 1994a.

Ray, R. D., B. V. Sanchez, and D. E. Cartwright, Some extensions to the response method of tidal analysis applied to TOPEX/Poseidon, *Eos Trans. AGU, 75* (16), Spring Meet. Suppl., 108, 1994b.

Ray, R. D., B. F. Chao, Z. Kowalik, and A. Proshutinsky, Angular momentum of Arctic Ocean tides, *J. Geod.*, in press, 1996.

Sasao, T., and J. M. Wahr, An excitation mechanism for the free 'core nutation', *Geophys. J. R. Astron. Soc., 64*, 729-746, 1981.

Schrama, E. J. O., and R. D. Ray, A preliminary tidal analysis of TOPEX/Poseidon altimetry, *J. Geophys. Res., 99*, 24,799-24,808, 1994.

Schwiderski, E. W., Ocean tides: A hydrodynamic interpolation model, *Mar. Geod., 3*, 219-255, 1980.

Seiler, U., Periodic changes of the angular momentum budget due to the tides of the world ocean, *J. Geophys. Res., 96*, 10,287-10,300, 1991.

Seiler, U., and J. Wünsch, A refined model for the influences of ocean tides on UT1 and polar motion, *Astron. Nachr., 316*, 419-423, 1995.

Sovers, O. J., C. S. Jacobs, and R. S. Gross, Measuring rapid ocean tidal Earth orientation variations with VLBI, *J. Geophys. Res., 98*, 19,959-19,971, 1993.

Wahr, J. M., Body tides on an elliptical rotating, elastic and oceanless Earth, *Geophys. J. R. Astron. Soc., 64*, 677-703, 1981.

Watkins, M. M., and R. J. Eanes, Diurnal and semidiurnal variations in Earth orientation determined from LAGEOS laser ranging, *J. Geophys. Res., 99*, 18,073-18,079, 1994.

Wilson, C. R., and R. O. Vicente, Maximum likelihood estimates of polar motion parameters, in *Variations in Earth Rotation, Geophys. Monogr. Ser.*, vol. 59, edited by D. D. McCarthy and W. E. Carter, pp. 151-155, AGU, Washington, D.C., 1990.

B. F. Chao, J. M. Gipson, C. Ma, and R. D. Ray, Laboratory for Terrestrial Physics, NASA Goddard Space Flight Center, Greenbelt, MD 20771. (e-mail: chao@denali.gsfc.nasa.gov)

G. D. Egbert, College of Oceanic and Atmospheric Sciences, Oregon State University, Corvallis, OR 97331.

(Received November 22, 1995; revised May 3, 1996;
accepted May 20. 1996.)